Dynamic Viscoelastic Modulus of Associative Polymer Networks: Off-Lattice Simulations, Theory and Comparison to Experiments

Robert D. Groot* and Wim G. M. Agterof

Unilever Research Laboratorium, P.O. Box 114, 3130 AC Vlaardingen, The Netherlands

Received December 28, 1994; Revised Manuscript Received May 25, 1995®

ABSTRACT: An off-lattice simulation model for associative polymer gels as introduced recently (Groot, R. D.; Agterof, W. G. M. *J. Chem. Phys.* **1994**, *100*, 1649) has been applied to obtain the mechanical spectrum as a function of frequency and polymer concentration, using a Green–Kubo relation for the time-dependent modulus. Two stages of relaxation are observable in our simulations. The early-time decay is consistent with a $-^2/_3$ power law, whose form is insensitive to large variations in polymer concentration, association lifetime, and degree of association. The late stage, which relaxes like the end-to-end vector in the Rouse model, has a characteristic stress that scales as the cube of the concentration and a relaxation time that is proportional to the monomer–monomer dissociation rate. The simulation results have been compared with experiments found in the literature for several physical gels. The quantitative agreement calls into question other postulated mechanisms involving hydrodynamic interaction or reptation, since the simulation contains neither of these features. As an alternative explanation for the observed early-time decay, an explicit relation between the power law exponent and the polymer fractal dimension is given.

1. Introduction

To characterize the rheologic behavior of soft condensed matter such as polymer solutions and polymer gels, often the dynamic modulus is measured. This modulus is a material property that relates the stress in a sample to its deformation. It can be obtained in two ways.[1] The first method is to use a step shear deformation. At $t = 0$ the sample is deformed as $(x, y, z) \rightarrow (x + \gamma y, y, z)$, where γ is a small strain. As a result of this deformation, the material responds with a shear stress σ, which usually damps out in time. Since the stress must be proportional to γ for small deformations, we have

$$\sigma(\gamma,t) = G(t)\,\gamma \tag{1}$$

The constant of proportionality, $G(t)$, is by definition the time-dependent modulus. Alternatively, the modulus can be obtained by imposing an oscillatory shear strain $\gamma(t) = \gamma_0 \sin(\omega t)$ on the system. The resulting stress is measured, which generally shows a phase shift, i.e.,

$$\sigma(t) = \gamma_0 G' \sin \omega t + \gamma_0 G'' \cos \omega t \tag{2}$$

The in-phase and out-of-phase constants of proportionality, the moduli G' and G'', depend on the frequency by which the sample is deformed and are related to the time-dependent modulus via the following Fourier transform:

$$G' + iG'' = i\omega \int_0^\infty e^{-i\omega t} G(t)\, dt \tag{3}$$

The linear modulus is also referred to as the mechanical spectrum. A schematic result found for the modulus of linear polymers[2] is shown in Figure 1. At very small frequency (the terminal zone) the modulus increases as $G' \propto \omega^2$ and $G'' \propto \omega$. At higher frequency the storage modulus approaches a constant, $G' = G_N^{(0)}$, the plateau modulus, and the loss modulus G'' decreases. From a certain point on G' increases again. A typical example for a polystyrene melt up to this frequency range is shown in Figure 4-4 by Larson;[1] the slope in the transition zone is roughly 0.63. This modulus increase is usually referred to as "glassy modes" because these are the only relaxation modes seen in a glassy state. The actual glassy zone is found at yet higher frequencies, where the storage modulus reaches a second plateau.

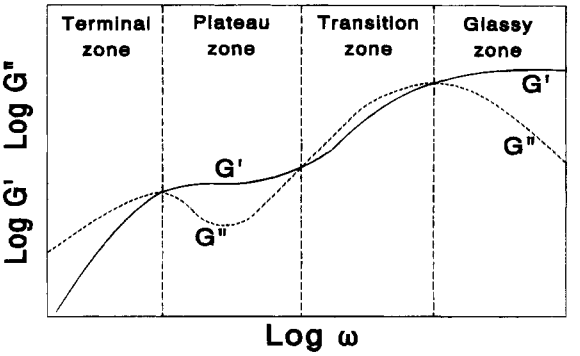

Figure 1. Schematic pattern of the complex modulus as a function of the frequency.

An important class of polymers cross-link in a reversible way, by a dynamic association equilibrium. The resulting structures are known as associative polymer networks. Some examples are synthetic polymers, such as modified polyacrylates,[3,4] poly(ethylene glycol) end-capped by long-chain alcohols,[5] hydrophobically modified guar,[6] and many biopolymers are known to form reversible networks.[7–10] The physical cross-link mechanism can be very different from one biopolymer to another, but on a macroscopic level many similarities appear, and the mechanical spectrum of these biopolymer networks very much resembles the general picture for (entangled) synthetic polymer melts as in Figure 1.

From this frequency dependence of the modulus, detailed conclusions can be drawn regarding the microstructure of the system. In this interpretation step, a (statistical mechanical) theory must be used that links a polymer microstructure to macroscopically observable quantities. Well-known are the Rouse and Zimm theo-

* Present address: Unilever Research Port Sunlight Laboratory, Quarry Road East, Bebington, Wirral L63 3JW, United Kingdom.
® Abstract published in *Advance ACS Abstracts,* August 1, 1995.

0024-9297/95/2228-6284$09.00/0

ries for isolated polymers (modeled as pointlike beads connected by springs) and the reptation theory,[11,12] which describes an ensemble of entangled polymers. Much progress has recently been made in applying the reptation model to associative polymer solutions:[13] the transition from the terminal zone to the plateau zone and the related time scales are understood quantitatively. However, quite some problems have remained that could not be solved by analytical theory.

To give a short summary, many associative polymers are found to phase-separate instead of forming a gel, when too many association sites are introduced on the polymer.[14] To fully understand this we must understand the phase diagram of these systems: when do the polymers form a gel, when is the system macroscopically unstable, and when does it form microdomains? A second set of questions relates to the mechanical spectrum: should one expect a single decay mode or a more complex reptation-like spectrum? What causes the minimum in G'' in the plateau zone? From the reptation model and related theories that account for the tube fluctuations this minimum is not understood.[1] What determines the modulus at short time, should one expect a Rouse spectrum ($G(t) \propto t^{-1/2}$) or rather a Zimm spectrum ($G(t) \propto t^{-2/3}$) that is dominated by hydrodynamics? How does the plateau modulus scale with polymer concentration? Classical network theory leads (at high polymer concentration) to $G_N^{(0)} \propto c^2$, whereas scaling theory suggests[11] $G_N^{(0)} \propto c^{2.3}$. For associative polymers the network relaxation time is observed to depend on the polymer concentration.[5] Can we understand this from a molecular picture? Finally, a third set of questions relates to the nonlinear rheologic behavior: can we predict, from a molecular basis, the transient behavior of associative gels under flow conditions? Which materials can be expected to show an apparent yield behavior?

As a proper analytic theory to answer these questions has not been developed yet, one may alternatively use a simulation method to analyze a microscopic model and derive a theory based on the trends observed in the simulations. One method utilized frequently is the Brownian dynamics method to solve the Langevin equation for a single chain.[15-17] This method is a very powerful tool to solve many questions concerning the rheology of the system, but there are some drawbacks. First, to correctly predict the finite viscosity at infinite frequency, an internal viscosity is attributed to the chains. There is no clear connection between this internal viscosity and the microscopic polymer structure. Second, because only the bond length distribution is calculated, all problems concerning thermodynamic stability and the concentration dependence of the rheologic properties are beyond this method.

To gain insight into the aspects mentioned, a simulation method should be employed that comprises an ensemble of polymer chains, which are represented by chains of atoms that all interact with each other via some interaction force. The atoms can be moved by several algorithms. First, Newton's equations of motion can be solved numerically. This is the molecular dynamics method. In the second method (Brownian dynamics), the Langevin equation is solved: each atomic velocity is proportional to the force acting on it, where the force includes a randomly fluctuating term. In the third method (Monte Carlo), the diffusion process through phase space is simulated by taking (small) random steps that are accepted or rejected according to the Metropolis algorithm. Using such an explicit representation of the polymers, the dynamics of cross-linking has been studied,[18,19] the crossover from Rouse diffusion to reptation diffusion has been followed,[20] and polymers in a Poiseuille flow have been studied.[21] The application of this simulation method to associative polymers has been described by us recently in two articles,[22,23] a similar model has been developed independently by Van den Brule and Hoogerbrugge.[24] In our first article[22] the thermodynamic behavior and the location of the sol-gel transition were studied, and in the second article[23] a qualitative picture of the (nonlinear) rheologic properties was given.

The Monte Carlo method employed here is the simplest possible continuum model of associative polymers; it contains only excluded volume interactions, a connectivity via Hookean springs, and of course the association and dissociation processes. Although lattice models are computationally more efficient than off-lattice models,[20] we have chosen this route, because in the continuum model one has full access to the stress tensor.[22] To gain computational efficiency, however, we have left out entanglement effects, hydrodynamic interactions, and conservation of momentum. Nevertheless, the model was shown to be qualitatively in line with experimental observation.[22,23]

To use this model for practical predictions the model must be mapped on experimental systems of interest, and therefore, it should be studied in a more quantitative way. As many experimental systems are characterized by their linear dynamic modulus, the mechanical spectrum has to be evaluated for this model; some preliminary results have been published before.[25] The simulated modulus is compared to a number of experiments, which led to insight in a number of questions that were posed above. In the next section we outline the simulation model and methods that we used. Special attention is given to the Green-Kubo relation, because this relation is crucial to understand the short-time divergence of the modulus. The actual simulation results are summarized in section 3, and compared to several experiments in section 4. In the last section, we give a speculation on the origin of the short-time divergence of the modulus and summarize our results and conclusions.

2. Simulation model and methods

2.1. Bead-Spring Model. In the model used the polymers are chains of L hard spheres, connected by harmonic springs. Each (free) sphere has a central association site, which can only be reached by another free atom via a Monte Carlo jump through the hard core. On association the energy increases by u_a. Once associated, the two spheres form a new spherical (united) atom, which is then connected by two, three, or four bonds to the networks, depending on the topological position of the original atoms. Because an explicit dissociation step must be taken to separate two associated atoms, the energy u_a can be either positive or negative. The only quantity of physical relevance is the association constant $K = V_a \exp(u_a/kT)$, where V_a is the volume that is scanned in search of a free partner.

To prevent reduction of the volume fraction on association, the hard-sphere diameter of a dimer relative to that of a single atom is larger by a factor of $2^{1/3}$. Thus we use the following interaction potential:

$$u_{ij} = \begin{cases} u^{HS}(r_i - r_j) + C(r_i - r_j)^2 \\ \quad \text{if } i \text{ and } j \text{ are neighbors in one chain} \\ u^{HS}(r_i - r_j) \\ \quad \text{otherwise} \end{cases} \tag{4}$$

where $i \neq j$ number the atoms, L is the polymer length, and the hard-core potential is given by

$$u^{HS} = \begin{cases} \infty & \text{if } |r_i - r_j| \leq d_{ij} \\ 0 & \text{if } |r_i - r_j| > d_{ij} \end{cases} \tag{5}$$

where $d_{ij} = a_i + a_j$, and $a_i = {}^1/_2$ for free atoms and $a_i = 2^{-2/3}$ for associated atoms. This simulation algorithm implies that only binary associations between the atoms are allowed. Unless stated otherwise, we shall use a total number of $N = 900$ spheres, and the fixed parameters $C = 0.3kT$, $L = 10$, and truncate the search for candidates for association at the distance $R_a = 1.2$. The system is periodic in all directions; the sizes of the box are $15 \times 15 \times 15$. The fraction of association–dissociation attempts was put at 10% in the present simulations. The 90% other Monte Carlo steps were attempted moves.

The attempted moves were taken from Gaussian distributions. For each direction (x, y, z) a random variable was generated from a standard normal distribution and multiplied by the mean step size. Two methods to determine the step size have been compared.

Method 1. For each individual atom, the mean fraction of accepted moves was measured. When this fraction was larger than 20% (this value leads to the fastest diffusion per MC step[26]), the step size was reduced by 1%; when it was smaller than 20%, the step size was increased by 1%. This algorithm led to a step size that fluctuated between 0.4 and 2.5 to give typical numbers. Because the fluctuations were rather slow (a period of some 250 MC steps), another method has been tried to find out whether these step size fluctuations lead to an artificial time scale in the simulation result.

Method 2. Again steps were taken from a Gaussian distribution, but now all atoms were moved by the same fixed mean step size $s = 0.68$, which leads to an overall mean acceptation fraction of 20%. Method 1, which optimizes the step size for each atom individually, may be a bit more efficient than the other method. A comparison of two long runs at the association energy of $6kT$ (850 000 MC steps per atom using method 1, and 1 000 000 MC steps per atom using method 2) shows a quantitative duplication of the stress autocorrelation function, both in the short-time domain (5–200 MC steps) and in the long-time domain (1000–40 000 MC steps); see Figure 2.

Remarkably, when the mean acceptation fraction in method 2 is measured per atom, a broad variation is observed from one atom to another. Over 1000 MC steps it varies from 11 to 36%; when the average is taken over 500 000 MC steps, still a variation from 16 to 27% acceptation is found. This suggests that the irregularities of the network structure for some atoms lead to a smaller diffusion constant than for others. If this is the case, the physical time that corresponds to a MC step is not simply proportional to the step size. If some atoms have a larger diffusion constant than others, these will acquire a larger mean step size in method 1. Consequently, one may not conclude that the physical time for these atoms runs faster than for others. If we accept the fact that the diffusion constant varies from one atom to another, then we are forced to take the number of collisions per atom as a measure of time. In that case, method 1, in which all atoms have exactly the same acceptation fraction (and hence collision rate), can be conjectured as the best representation of a physical system. However, as the two methods give exactly the same time correlation function, we are not forced to make a conceptual choice for one method over the other.

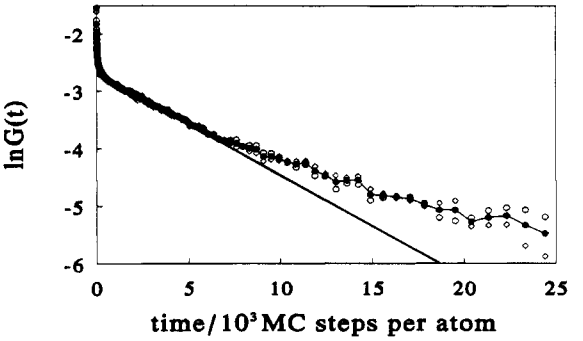

Figure 2. Logarithm of the time-dependent modulus as a function of time for $u_a = 6kT$. Open symbols are independent runs using simulation methods 1 and 2.

2.2. Green–Kubo Relation. The most straightforward way to obtain transport coefficients like the shear viscosity from a simulation is to apply an external field that will move the atoms;[23] the ratio of the applied force and the resulting shear rate by definition equals the shear viscosity. Applying an oscillatory external field would result in the frequency-dependent moduli. There are two disadvantages of this method. First, for each desired frequency, a new simulation must be run; this leads to a large amount of necessary simulation time. The second disadvantage of this method is that the external field must be very weak to ensure that the linear response of the system is measured. As a check, simulations at several external field strengths must be done to find the regime of *linear* viscoelasticity. The way around these disadvantages is to use the fluctuation–dissipation theorem. This theorem enables one to obtain the frequency-dependent moduli for all frequencies from a single simulation and was used quite some time ago,[27] but it has not been used all that much since then. Because our results crucially depend on the validity and applicability of this theorem, and because we feel that the power of this method has not been appreciated enough, we give a short outline of the method here, where we closely follow the derivation by Doi and Edwards.[11]

Consider a time-dependent external field $\gamma(t)$ deforming a sample such that the shear stress σ_{xy} will have a finite value (γ is the mean shear deformation relative to the equilibrium configuration; γ and σ_{xy} are conjugate variables). For all times $t < 0$ the field is constant, $\gamma(t) = \gamma$, and at $t = 0$ the field is switched off, $\gamma(t) = 0$ for $t > 0$. At negative times the stress is proportional to γ:

$$\sigma_{xy} = G\gamma \tag{6}$$

We achieve this stress increase by adding the following potential to the Hamiltonian:

$$U_{ext} = -V\gamma(t)\sigma_{xy} \tag{7}$$

The total work performed on building up the stress is

$$W = V\int_0^\gamma \sigma_{xy}\,d\gamma' - V\gamma\sigma_{xy}$$
$$= {}^1/_2 VG\gamma^2 - V\gamma\sigma_{xy} = (V/2G)\sigma_{xy}{}^2 - V\gamma\sigma_{xy} \quad (8)$$

As the system will tend to minimize the total free energy, the equilibrium value of σ_{xy} is found upon minimizing eq 8 with respect to the stress. This does indeed lead to the stress given in eq 6; hence the external potential eq 7 is indeed the correct one.

At times $t > 0$, the stress will relax to its new equilibrium value $\langle\sigma_{xy}\rangle_0 = 0$ (a subscript γ at average brackets will be used to indicate an ensemble average where the external field is put at the value γ), and if the imposed deformation γ is small, the mean value during the relaxation process will be a linear functional of the field: (see also eq 1).

$$\langle\sigma_{xy}(t)\rangle_\gamma = \int_{-\infty}^t \mu(t-t')\gamma(t')dt' \equiv G(t)\,\gamma \quad (9)$$

Now $\langle\sigma_{xy}(t)\rangle_\gamma$ can be calculated if we know the distribution function $\psi(x^N,t)$, which is the probability of finding the system at the position $x^N = (x_1, x_2, ..., x_N)$, at time t. The result is

$$\langle\sigma_{xy}(t)\rangle_\gamma = \int \sigma_{xy}(x^N)\,\psi(x^N,t)\,dx^N \quad (10)$$

where $\sigma_{xy}(x^N)$ is the microscopic expression for the xy component of the stress tensor.

To find the time-dependent distribution function we first realize that no field is present for $t > 0$. Therefore, the time evolution of the system is given by the evolution operator *in the absence* of the field. Thus, the evolution is found from the Green function $G(x^N,x'^N;t)$, which describes the diffusion process from point x'^N at $t = 0$, to the point x^N at time t:

$$\psi(x^N,t) = \int G(x^N,x'^N;t)\psi(x'^N,0)\,dx'^N \quad (11)$$

Since at $t = 0$ the distribution is still at equilibrium with the situation where the external field was present, the distribution is then given by

$$\psi(x'^N,0) = \frac{\exp[-U(x'^N)/kT - U_{ext}(x'^N)/kT]}{\int\exp(-U/kT - U_{ext}/kT)\,dx''^N}$$
$$\approx \frac{\exp[-U(x'^N)/kT](1 + V\gamma\sigma_{xy}(x'^N)/kT)}{(\int\exp(-U/kT)\,dx''^N)(1 + V\gamma\langle\sigma_{xy}\rangle_0/kT)}$$
$$= \Psi_{eq}(x'^N)[1 + V\gamma\sigma_{xy}(x'^N)] \quad (12)$$

where the approximation holds for a very weak external field and where ψ_{eq} is the (equilibrium) distribution at zero field. If we now combine the last four equations, we find the time-dependent modulus as

$$G(t) = \int\int \sigma_{xy}(x^N)G(x^N,x'^N;t)\,\psi_{eq}(x'^N)[1 + V\gamma\sigma_{xy}(x'^N)/kT]\,dx^N\,dx'^N$$
$$= \langle\sigma_{xy}\rangle_0 + V\gamma\int\int \sigma_{xy}(x^N)G(x^N,x'^N;t)\psi_{eq}(x'^N)\sigma_{xy}(x'^N)/kT\,dx^N\,dx'^N$$
$$= \frac{V\gamma}{kT}\langle\sigma_{xy}(t)\sigma_{xy}(0)\rangle_0 \quad (13)$$

where again the fact has been used that the mean value of the shear stress is zero at vanishing field. Now the external field appears at the left- and right-hand sides of the equation; hence it drops out. At zero external field, we therefore have a relation between the time-dependent modulus and the time correlation function of the (spontaneous) fluctuations of the shear stress.

It should be noted that nowhere in this derivation has an explicit expression for the Green function been used. Therefore, it may be used in any type of simulation method, no matter whether molecular dynamics (integration of Newton's equation), Brownian dynamics (integration of the Langevin equation), or Monte Carlo (random steps are taken following the Metropolis algorithm) is used. Furthermore, nowhere in the derivation has the interaction potential between the atoms been used. Therefore, the method is valid even though the interaction energy between neighboring atoms on a chain increases with separation; i.e., the method is valid for polymers. Another relevant point to mention is that the derivation is based on the notion of a state Ψ_{eq}, which in a *statistical* sense is stationary to infinitesimal distortions. This does *not* mean that Ψ_{eq} should be a true thermodynamic equilibrium state. The only relevant issues are that the simulation method generates the correct diffusive motion of the system through phase space and that Ψ_{eq} is sufficiently isotropic so that $\langle\sigma_{xy}\rangle_0 = 0$. Systems in a metastable state, like a microphase-separated gel or a glass, evolve very slowly on a global scale but make frequent excursions from the stationary state and back again on a much shorter time scale. The implication of the theorem is that these excursions determine the dynamic modulus of the system on a time scale that is short as compared to the time scale of global evolution. All present simulations meet these conditions.

The derivation given here is only one example of the more general fluctuation–dissipation theorem, which was introduced by Green[28] and Kubo.[29] Therefore the identity given in eq 13 is usually referred to as a Green–Kubo relation, though several others have contributed to this theory. An excellent overview of the method and its numerous applications was given by Zwanzig.[30]

2.3. Short-Time Divergences and Fourier Transform. One direct application of the Green–Kubo relation can be found when the frequency-dependent moduli are studied in the limit $\omega \to \infty$. This limit naturally is related to the time correlation function at $t = 0$, i.e., the instantaneous fluctuation amplitude. This amplitude is determined by the equilibrium structure of the liquid only. Zwanzig and Mountain[31] used this fact to derive a generally valid expression for the high-frequency limits of the shear modulus and the bulk modulus in terms of the pair correlation function, for liquids with a central two-body potential $u(r)$. For these systems the internal energy density, the pressure, and the infinite frequency shear modulus are given by

$$\langle u\rangle = \frac{3}{2}\varrho kT + 2\pi\varrho^2\int_0^\infty dr\,g(r)r^2u(r) \equiv \frac{3}{2}\varrho kT + 2\pi\varrho^2 I_1 \quad (a)$$

$$p = \varrho kT - \frac{2\pi}{3}\varrho^2\int_0^\infty dr\,g(r)r^3\frac{du}{dr} \equiv \varrho kT - \frac{2\pi}{3}\varrho^2 I_2 \quad (b)$$

$$G'_\infty = \varrho kT + \frac{2\pi}{15}\varrho^2\int_0^\infty dr\,g(r)\frac{d}{dr}\left(r^4\frac{du}{dr}\right) \equiv \varrho kT + \frac{2\pi}{15}\varrho^2 I_3 \quad (c)$$

(14)

Now let us apply these identities to a system of soft spheres with interaction potential $u(r) = (a/r)^m$. In that case we have $u'(r) = -ma^m/r^{m+1}$ and $u''(r) = m(m+1)a^m/r^{m+2}$. The first integral ($a$) appearing in eq 14 is now given by $I_1 = a^m \int g(r)/r^{m-2}\, dr$. From a few simple algebraic manipulations we directly find the other integrals to be proportional to I_1. Explicitly, we have $I_2 = -mI_1$ and $I_3 = m^2 I_1$. If we now study the limit $m \to \infty$, the interaction potential describes a hard-sphere system. For this system, the pressure is a finite number; hence I_2 is a finite number (for low density it reduces to the second virial coefficient, up to a factor $2\pi/3$). The consequence is that the internal energy is proportional to $1/m$ (hence it is zero) and the modulus is proportional to m; hence *the infinite frequency modulus for hard spheres is infinitely large*. This fact is a direct consequence of the fact that the interaction force diverges at contact. Such a divergence of the infinite frequency modulus with the power m has been found recently by Heyes and Mitchell, who applied the Green–Kubo method to the modulus of a colloid suspension.[32]

This divergence is experimentally found for silica in cyclohexane by Van der Werff et al.,[33] who found $\eta^*(\omega) - \eta^*(\infty) \propto \omega^{-1/2}$ over three decades. This slow decay of the complex viscosity implies $G^*(\omega) - \omega\eta^*(\infty) \propto \omega^{1/2}$ as $\omega \to \infty$, in line with theories on the linear viscoelastic behavior of hard-sphere liquids[34,35] that neglect the hydrodynamic interactions. This fact apparently is in contrast with the result from Russel and Gast,[36] who found the hydrodynamic interaction to induce a decay $\eta^*(\omega) - \eta^*(\infty) \propto \omega^{-1}$, and with the conjecture of Brady,[37] who removed the divergence by hand, because it would be unphysical. The $\omega^{1/2}$ divergence for the hard-sphere system, however, can be understood quite easily; a simple analysis is given in our Discussion section. For polymer gels, the exponent may differ from $^1/_2$; therefore, we define for the general case an exponent n that describes the divergence:[38–40]

$$G^*(\omega) \propto \omega^n \tag{15}$$

in the high-frequency limit.

The $t \to 0$ divergence of the time-dependent modulus has direct consequences for the way the Fourier transform has to be calculated. In the simulation, the pressure tensor is measured via the virial equation.[22] The density–density correlation is measured via its first moment because this moment appears to vary only very little with r. Because the shear components of the pressure vanish on the average, the pair correlation function is simply averaged over a bin of width $(2^{1/3} - 1)/2 \approx 0.13$. This choice originates from the fact that two atom diameters are present, 1 and $2^{1/3}$, and that only one overall correlation function is measured; the contact values follow from the discontinuities in this overall $g(r)$. Whenever the surfaces of two atoms are within the distance 0.13, they are counted as to contribute to the contact value of the pair correlation function. Because the volume over which the contact density is measured is finite, the instantaneous fluctuations in the contact density are finite also. Only when the bin size would vanish would this instantaneous density vary between 0 (no atoms in the volume) and ∞ (1 atom in the volume), and infinite fluctuations in the $t = 0$ modulus would be found. Because a finite bin size excludes the divergent $t = 0$ fluctuations, the shear stress autocorrelation function must be extrapolated to $t = 0$ in a smart way to obtain the correct Fourier transform.

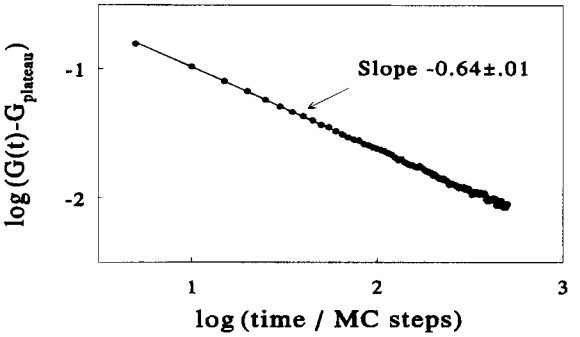

Figure 3. Short-time modulus showing algebraic decay over two decades. The plateau modulus is subtracted ($u_a = 6kT$).

The following procedure was used. The logarithm of $G(t)$ is plotted against time (open symbols) as in Figure 2 for the two simulation methods; the closed symbols give the logarithm of the average of the two runs. No smoothing has been used in this plot; it represents the raw data. The first strong decrease in $G(t)$ results from the $t \to 0$ divergence. The long-lived network connections are responsible for the long-time correlation. The two physical mechanisms [(i) the hard-sphere collisions and (ii) the network connectivity] lead to two additive contributions to the modulus. Therefore the long-time behavior is extrapolated to $t = 0$ by a single exponential, (this value is the plateau modulus) and subtracted from the measured $G(t)$. The difference is the short-time modulus, which has been plotted on a log–log scale against time; see Figure 3. The short-time modulus appeared to follow a straight line; the slope by definition equals $-n$. For several runs it was found that $n \approx {}^2/_3$ is a good approximation; hence to obtain the correct Fourier transform, the measured $G(t)$ was fitted to a function of the form $a + bt^{-2/3}$. This function was Fourier transformed between $t = 0$ and $t = 5$ and added to the numerical Fourier transform of $G(t)$. This numerical transform was obtained by interpolating $G(t)$ between successive points by a straight line. The analytic Fourier transforms over these intervals were added. Beyond the last point $G(t)$ is extrapolated to zero, and the Fourier transform over this part is added to the result. If no extrapolation is used, the complex modulus shows some artificial oscillations at small ω. A straight line extrapolation largely removes this artifact, but some further noise reduction is obtained when $G(t)$ is extrapolated by a single exponential or by a function of the form $\exp(-a(t^{1/2}))$. This latter form was used because $G(t)$ at long time is not a single exponential; see Figure 2. It has been determined that the use of this extrapolation method does not artificially bias the results; the added part is sufficiently small.

3. Simulation Results

3.1. Frequency Dependence. At one density, $\varrho = 0.2667$, the bead-spring model has been simulated for two values of the association energy ($u_a = 6kT$ and $u_a = 8kT$) to find the general frequency dependence of the model. Furthermore, the simulation method was checked by duplicate runs. For the $6kT$ system 850 000 MC steps per atom were taken using method 1, and 10^6 using method 2. For the $8kT$ systems, these numbers are 2×10^6 and 3×10^6 respectively. For the $8kT$ system, methods 1 and 2 led to different results: using method 1, the relaxation time was larger than the relaxation time obtained with method 2 by a factor of 3. A possible explanation could be that in method 1 the

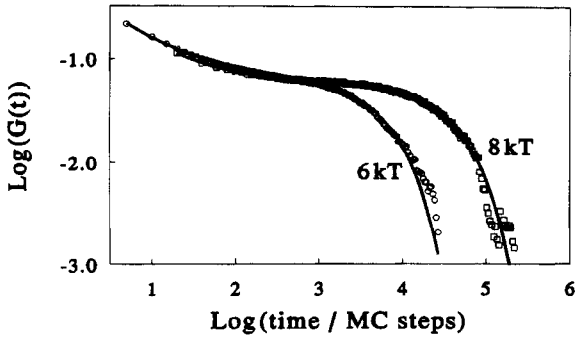

Figure 4. Simulated modulus for two sticker lifetimes. The smooth curves are fits to the power law plus terminal relaxation processes.

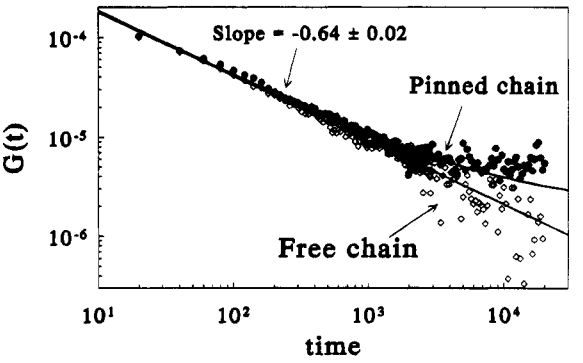

Figure 5. Modulus as a function of time for a pinned chain (closed symbols) and a free chain (open symbols).

atoms do not diffuse away from each other as efficiently as in method 2 after dissociation, and a large fraction reassociates again. This would lead to a longer effective sticker lifetime. For the $6kT$ system, however, the two methods gave identical results. The density dependence of the modulus was studied only at the association energy $u_a = 6kT$; first we concentrate on the modulus at a fixed density.

These results are shown on a log−log scale in Figure 4 (only method 2 for the 8kT system). In all cases, the short-time decay of the modulus was analyzed by subtracting the plateau modulus from $G(t)$. To obtain the best estimate of the plateau value, it was varied such that the short-time modulus would follow a straight line in a log−log plot, as in Figure 3. For both $8kT$ systems this led to an estimated exponent $n \approx 0.68 \pm 0.04$. At $6kT$ a better accuracy is obtained, because these systems relax faster. For the first $6kT$ run, the exponent was estimated as $n \approx 0.66 \pm 0.02$; the combined results of the two $6kT$ runs gave $n \approx 0.64 \pm 0.01$. These differences are considered not to be significant.

This result leads to the remarkable observation that the high-frequency divergence of the modulus is reasonably well described by the Zimm model ($n = {}^2/_3$). However, the Zimm model is essentially based on the assumption that the hydrodynamic interaction is dominant and that the finite volume effects are negligible ($n = {}^2/_3$ was calculated for θ polymers). However, in the simulations presented here, no hydrodynamic interactions at all have been taken into account. This brings us to the question why we have this apparent Zimm behavior ($n \approx {}^2/_3$). Are the constraints caused by the associations (i.e., the fixed topology) responsible for this deviation from the (expected) Rouse behavior ($n = {}^1/_2$) or are the finite volume effects in some way responsible?

To answer this question, the simulation system has been simplified to *one* chain of length $L = 100$, which was *not* allowed to associate and which was enclosed in a box of volume $V = 75 \times 75 \times 75$. This is the dilute limit; the system is too large for the chain to interact with its mirror images. To mimic the topological constraints, atoms number 10, 30, 50, 70, and 90 were not allowed to move after a first equilibration run of 10^5 steps/atom. Next, 10^6 steps/atom were taken, and the shear stress was measured. This chain will be referred to as "pinned".

In a control experiment, the constraints were released, and another 10^6 steps/atom were taken for this free chain. The results of these runs are shown in Figure 5. This graph shows that the modulus of the pinned chain reaches a plateau by a correlation time of 3000 MC steps/atom, whereas the modulus of the free chain decreases further. At shorter time, no difference between the two systems is found, apart from a small increase of the modulus of the pinned chain relative to the free chain. This difference is considered not to be significant. The modulus of the pinned chain is now fitted to a function of the form $a + bt^{-n}$; for the free chain the first term is put at zero. There is a systematic trend in the first few points to lie below the straight line of the overall trend; therefore, the result for the exponent n depends somewhat on the number of points that are discarded for the fit. This variation, however, is smaller than the estimated error in the fit parameters. This way it was found that for the pinned chain $n = 0.656 \pm 0.026$, and for the free chain $n = 0.637 \pm 0.008$. As the differences are within the estimated errors, the exponents are to be considered equal. It is therefore concluded that the value of the exponent n is determined by the excluded-volume interactions of the hard spheres and not by the topological constraints, frozen degrees of freedom, or hydrodynamic interaction.

The excluded-volume interactions in chain molecules are known to give rise to a lower fractal dimension ($d_f = 1.7$) than that of ideal coils ($d_f = 2$). Therefore we conjecture that the value of the exponent n is related to the fractal structure of the polymer. Such a notion has been put forward before by Martin *et al.*[39] and by Muthukumar.[40] In the Discussion section, an alternative derivation is given. To support this relation, both n and d_f have to be determined independently, which has been done in a second control experiment. Again a free chain of length $L = 100$ has been simulated over 2×10^6 MC states/atom, but now we used the second simulation method, with a fixed step size 1. The Fourier transform of the density was averaged for wave vectors parallel to the system axes. This led to the structure function $S(k) = \langle \varrho(k)\varrho(-k)\rangle/L - 1$ that is shown in Figure 6. When we simply fit a straight line through the first three points, we find a slope -1.78 ± 0.03. At higher k values the slope gets more negative, which is caused by the hard-core structure function $S^{HC}(k) \sim (\sin(k)/k - \cos(k))/k^2$. A fit to the sum of a power law and this function led to a power -1.70. Since the result depends on details of how the fit was made (two examples are shown in Figure 6), we cannot give a more accurate estimate than $d_f = 1.75 \pm 0.05$. For the stress correlation we find a somewhat lower exponent at short time scale than at longer time scale. Between $t = 20$ and $t = 200$ we find $n = 0.50 \pm 0.01$, and between $t = 200$ and $t = 8000$ we find $n = 0.616 \pm 0.016$. Although this value is a bit lower than that obtained in the previous runs, we consider the difference not to be statistically significant.

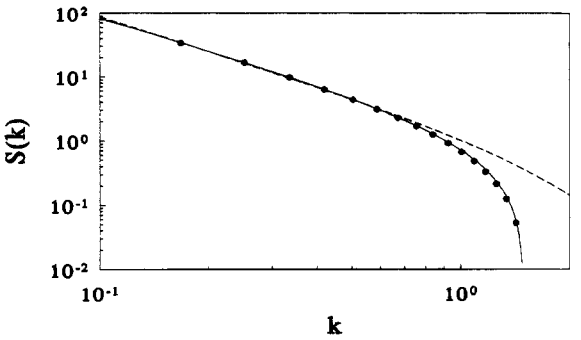

Figure 6. Structure function of an $L = 100$ polymer at fixed MC step size. The dashed curve extrapolates to a slope $d_f = 1.8$; the full curve leads to $d_f = 1.7$.

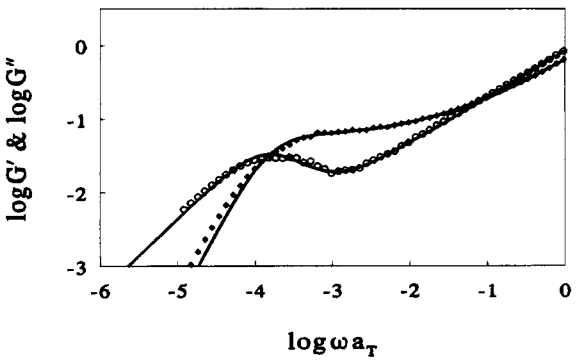

Figure 7. Complex modulus of the $6kT$ system. The curves show the terminal relaxation plus power law fit.

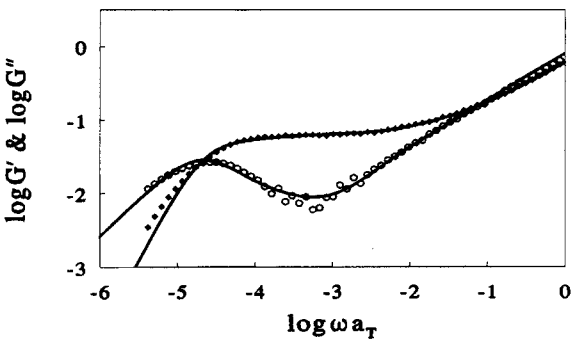

Figure 8. Complex modulus of the $8kT$ system. The curves show the terminal relaxation plus power law fit.

Another unexpected result is found when the long-time behavior of the system is studied. From Figure 2 it clearly follows that the stress autocorrelation is not a single exponential. This is also apparent when the Fourier transform $G^*(\omega)$ is studied (Figures 7 and 8). For the $8kT$ system this nonexponential character is even more pronounced, because the plateau time (the sticker lifetime) is much longer than it is in the $6kT$ system. The loss modulus of the $8kT$ system in Figure 8 between $\log(\omega) = -4.5$ and $\log(\omega) = -3.5$ decays with a power -0.45 ± 0.1 instead of the power -1 that a single-exponential decay would give. A power -0.5 also comes forward in the reptation theory, where it is related to the diffusion of chain ends into their tube.

The fact that we find this power of course does not prove that the reptation mechanism is relevant here. In fact, the present model allows all bonds to cross; hence no polymer in this simulation is confined to a tube. What this simulation does show is that the relaxation process is not determined by the lifetime of a single bond. In other words, the stress that a bond carries is only partially released on dissociation. Most probably it is transferred to the direct neighbours in the network and only diffuses away slowly by the breaking of other bonds. It is a peculiar observation that this stress relaxation is so well in line with the reptation theory.

On the basis of these results it is to be expected that the full modulus can be described by a sum of two basic relaxation processes. To show this, the data were fitted to a four-parameter function:

$$G(t) = FG_p(t/\tau_p) + G_N^{(0)}G_t(t/\tau_t) \tag{16}$$

where $G_p(t)$ describes the early-stage power law behavior and is approximated by the Zimm modulus,[11]

$$G_p(t) = \sum_{p=1}^{\infty} \exp(-p\sqrt{p}\, t) \tag{17}$$

and $G_t(t)$ describes the terminal relaxation and is approximated by the reptation spectrum[41]

$$G_t(t) = \frac{8}{\pi^2} \sum_{\text{p odd}} \frac{1}{p^2} \exp(-p^2 t) \tag{18}$$

The real-time fits are also shown in Figure 4, the (analytical) Fourier transforms of the same fits are shown in Figures 7 and 8. The resulting fit parameters for the $6kT$ system give the time scales $\tau_p = 127$ and $\tau_t = 6.8 \times 10^3$ and the moduli $F = 0.019$ and $G_N^{(0)} = 0.077$. For the $8kT$ system, we found $\tau_p = 100$ and $\tau_t = 4.7 \times 10^4$, and the moduli $F = 0.021$ and $G_N^{(0)} = 0.068$. The error in the moduli and τ_t can be estimated at 5−10%; the uncertainty in τ_p is some 20%.

The terminal relaxation time scale τ_t is proportional to the life time of a sticker: an energy increase of $2kT$ does indeed lead to an increase in the relaxation time by a factor $7 \approx e^2$, whereas the power law time scale τ_p below which the glassy modes become important is roughly independent of the sticker lifetime. When the terminal spectrum G_t in eq 16 is replaced by a single exponential, the root-mean-square deviation of the fits do not change by much, but the best fits are now obtained for $\tau_p = 1460$ and $\tau_p = 32\,000$ respectively, i.e., power law time scales comparable to the terminal relaxation time. The deviation from a single exponential is thus described by an unrealistically extended power law spectrum. Inspection of the data in Figure 8 (or Figure 4) shows that indeed the plateau is reached by $t \approx 100$; hence we must discard the single-exponential model in favor of the "reptation" spectrum, which describes the data quantitatively.

3.2. Density Dependence. A more detailed picture of the system is obtained when the density dependence is studied. For practical reasons, only the weak gel at $6kT$ is studied for the densities given in Table 1. The results of these simulations are shown in Figure 9 for the densities $\varrho = 0.0533$, 0.08, 0.1185, 0.1777, and 0.2666. To analyze these data, eq 16 was used again as a fit equation. It should be mentioned here that the mean-square deviation of the fit to the data appears to vary only little with τ_p. Therefore, only $G_N^{(0)}$, F, and τ_t were used as free fit parameters, and τ_p was kept fixed. Next, τ_p was varied by hand and a new (three-parameter) fit was made; until the total square deviation was minimized. For the $\varrho = 0.1777$ and $\varrho = 0.2222$ systems, no minimum in the square deviation was found for realistic values of τ_p. The values given in Table 1 are chosen as a reasonable guess. The numerical value

Table 1[a]

ϱ	$p \times 10^3$	$-\Delta p \times 10^3$	$F \times 10^3$	$G_N^{(0)} \times 10^3$	τ_p	τ_t	τ_a	s	α
0.053	1.6	8.4	1.2	1.0	365	1660	10 600	0.687	0.964
0.080	2.2	18	1.8	3.5	385	2540	10 700	0.804	0.966
0.119	1.3	41	2.3	12.2	550	3760	11 100	0.957	0.968
0.178	2.9	93	7.0	40.5	200[b]	5690	9 600	0.991	0.972
0.222	10.8	143	9.6	57.0	200[b]	6330	11 600	0.997	0.975
0.267	28.1	201	17.3	76.5	123	6725	11 700	0.999	0.977

[a] p, pressure; Δp, network excess pressure and moduli ($\times 10^3$), relaxation times (MC steps); s, cluster size/system size; α, fraction of associated atoms. The error in the pressure varies from 0.2 at low density to 0.6 at the highest density. [b] No least-square minimum was found on variation of τ_p; these values are estimated.

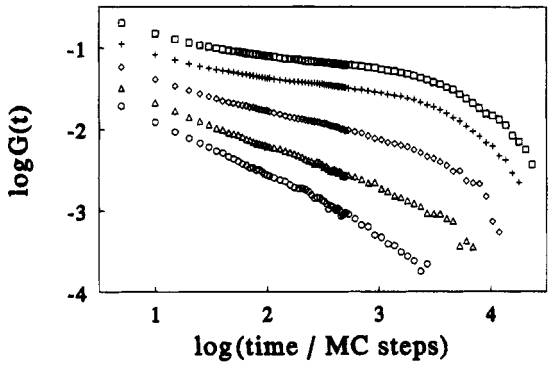

Figure 9. Time-dependent moduli for several densities. From top to bottom the density decreases by a factor 1.5 for each next system.

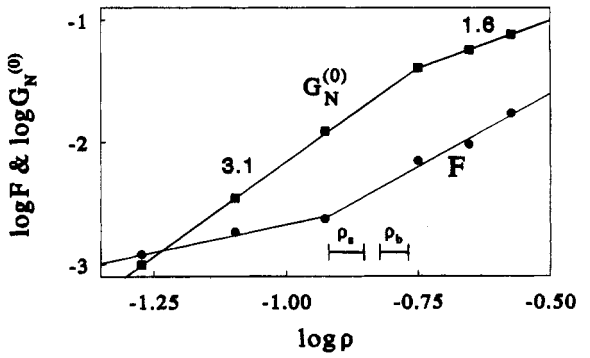

Figure 10. Plateau modulus ($G_N^{(0)}$) and glassy modulus (F) as a function of density. The slopes are indicated by the numbers. The error bars give the upper spinodal and binodal densities.

of $G_N^{(0)}$ is rather insensitive to the choice of τ_p, but F varies by 30% when τ_p is varied from 130 to 300.

Apart from this uncertainty in F, a good correlation between the modulus and the density is found, as shown in Figure 10. At low concentration the plateau modulus and glassy modulus are found to scale roughly as

$$F \propto \varrho \quad \text{and} \quad G_N^{(0)} \propto \varrho^{3.1\pm0.1} \tag{19}$$

Lines of slope 1 and slope 3.1 at low concentration have been added to the plot. At higher concentration a crossover to a different slope is found; the slope of F increases. The slope in $G_N^{(0)} \approx 1.6 \pm 0.2$ does not seem to be consistent with a slope 2.3, which is expected from the scaling behavior of free polymers. The slope 1.6, however, is in line with a rigid rod network model. For flexible cross-links, field theory predicts $G \propto \varrho^{3/2}$, and for frozen cross-links, $G \propto \varrho^2$ is derived.[42]

The pressure, which has been measured simultaneously, shows a clear van der Waals loop: when the density increases it goes up, down, and up again (see Table 1). By fitting the pressure to the virial expansion $p/kT = \varrho/10 + a\varrho^2 + b\varrho^3$, the binodal densities $\varrho = 0.029 \pm 0.004$ and $\varrho = 0.16 \pm 0.01$ are found. The upper spinodal and binodal densities are indicated in Figure 10. It is now observed that the range where the slopes 1 and 3.1, respectively, are pertinent to the moduli corresponds to the range of (micro)phase separation. As the plateau modulus over this density range shows a smooth ϱ^3 increase, apparently, the proportionality $G_N^{(0)} \propto \Pi_{osm}$ is *not* correct for (micro)phase separating gels. The network excess pressure (i.e., the difference with the pressure at zero association constant) varies as $\Delta p \propto \varrho^{2.03}$; hence also the relation $G_N^{(0)} \propto \Delta p$ does not hold.

Another relevant issue is the dependence of the terminal relaxation time with concentration. Over the concentration range studied, it varies significantly; see Table 1. To a very good approximation it scales linearly with the polymer concentration:

$$\tau_t \propto \varrho \tag{20}$$

Only for the highest two densities does this proportionality not hold; here the network relaxation time approaches the lifetime of the stickers and tends to level off.

Intuitively, it seems obvious that this dependence of the terminal network relaxation time on the polymer concentration is caused by some structural effect of the gel. To be certain of this, two questions should be answered. First, is the intrinsic lifetime of an associate indeed independent of the concentration, and secondly, does the topological structure of the gel indeed change significantly over this range of concentrations? The first question can be solved from the recorded number of accepted dissociation attempts. The total number of MC states divided by this number gives a reasonable estimate of the lifetime of an associated pair τ_a, which is also shown in Table 1. However, in principle, individual pairs of atoms could dissociate from and associate to the same partner several times. This would increase the effective lifetime of the association. Therefore we also measured the correlation function of association between individual atoms in small separate runs (5×10^4 MC states/atom). We found single-exponential decays. The lifetime of an associate estimated from these correlation functions corresponds to the earlier estimates to within 10–20%. Any differences found are far too small to explain the differences in the terminal relaxation times τ_t.

To answer the second question, the cluster size distribution functions were measured over the same runs that were used to obtain the stress correlation. The mean cluster size divided by the system size (s) is given in Table 1. At low concentration the mean cluster size clearly drops, as the percolation transition is approached. The fraction of associated atoms (α in Table 1), however, does not change dramatically. This means that the polymers tend to exchange intermolecular associations in favor of more intramolecular associa-

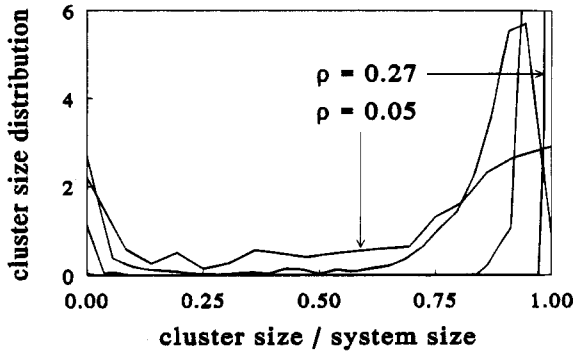

Figure 11. Cluster size distribution functions for the systems shown in Figure 9, at densities ϱ = 0.053, 0.080, 0.119, and 0.267. The lowest densities approach the sol–gel transition point, but are still in the gel phase.

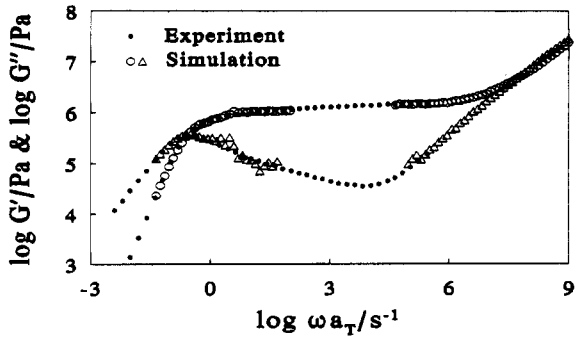

Figure 12. Experimental data of a polybutadiene melt (full symbols) and Monte Carlo data (open symbols). The experimental data was read off Figure 4-5 of ref 1. The high-frequency simulation data are frequency shifted to fit the high-frequency part of the experiment.

tions. This approach of the sol–gel transition in visualized more clearly by the cluster size distributions shown in Figure 11. At the lowest concentration, a very broad cluster size distribution is visible (indicating the proximity of the sol–gel transition point). Nevertheless this system is a (weak) gel because a significant gel peak is visible. As the concentration increases, the distribution continuously shifts toward full (100% connection) and stronger gels.

4. Comparison between Simulation and Experiment

4.1. Frequency Dependence. A crucial test of the simulation model, of course, is a comparison with experimental data. In Figure 12, the $8kT$ system simulated with method 1 (which has the longest network relaxation time) has been compared to the experimental moduli of polybutadiene of molecular weight 360 000 and narrow polydispersity. This data was taken from Larson,[1] (p 103, Figure 4-5). The MC data clearly show very good agreement with the experimental data in the low-frequency range: the terminal zone and the plateau zone up to the point where the glassy modes start off in the simulations. The slope in the decreasing part of G'' seems a bit steeper than the experimental value (-0.45 ± 0.1 rather than -0.31), but still the deviations may be attributed to the noise in the simulations. The important thing here is that the two relevant time scales τ_p and τ_t, are sufficiently far apart in the simulations that we can distinguish between the two processes. By frequency shifting the high-frequency simulation results (and applying a small vertical shift), we are able to compare the glassy mode part of the simulated spectrum with the experiment. This comparison is also made in Figure 12: the simulations capture the upturn of G'' and the correct slope is predicted.

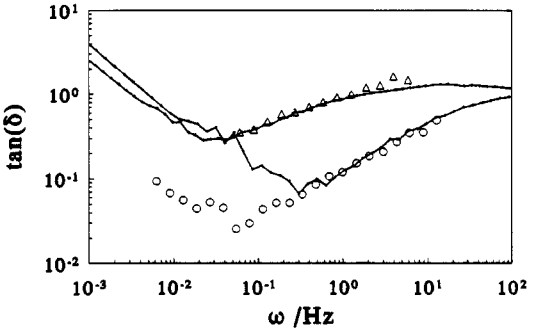

Figure 13. Gelatin loss angle (triangles 0.8%; circles 0.9%) reproduced from Carnali[10] (Figure 4). The curves give the $6kT$ and $8kT$ simulation results, frequency shifted to fit the glassy modes.

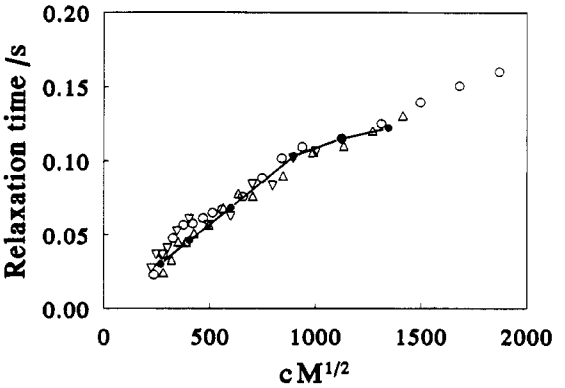

Figure 14. Network relaxation time of end-capped associative polymers, from Annable *et al.*[5] (Figure 7). Open symbols, experiments; curve and closed symbols, simulation.

Another example is the frequency dependence of gelatin. The ratio of G'' to G' defines the loss angle, which is shown in Figure 13 for gelatin. The data were read off Figure 4 from Carnali.[10] For comparison, the frequency-shifted simulation results for tan δ ($=G''/G'$) of the $6kT$ and the $8kT$ systems are added. Clearly, the curves compare quantitatively with the gelatin data. Note that the 0.9% data in Figure 13 imply a distinct minimum in G'', just as the simulations and the polybutadiene data of Figure 12 do. The fact that this minimum in tan δ does not coincide with the simulated value is simply caused by the limited sticker lifetime that we can simulate in a reasonable time.

4.2. Concentration Dependence. The concentration dependence of the network relaxation time was reported by Annable *et al.*[5] They studied a model system of associative polymers comprising poly(ethylene glycol) (PEG), end-capped by long-chain alkanols. In this system, the polymers only stick at the end points because the alkanol chains tend to form micelles. The network relaxation time has been measured for a number of PEG molecular weights and polymer concentrations. The length of the alkanol chain (i.e., the sticker lifetime) was kept fixed. These results are reproduced in Figure 14. For this model system, the relaxation time does vary with concentration, and to a reasonable approximation, a linear scaling with concentration was found, as predicted by the present simulation model (eq 20). Both experiments and simulations show a tendency to level off at higher concentration. The simulations have been fitted to the experiments by rescaling the concentration and the time axis

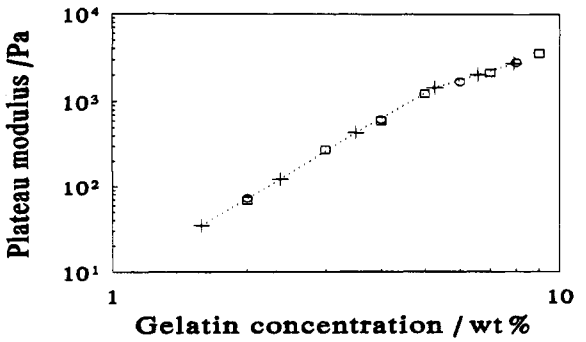

Figure 15. Gelatin modulus by Carnali[10] (squares) and Bot[43] (circles) as compared to the simulation results (crosses connected by dotted lines).

of the simulation data. The actual prediction is therefore not this slope, but merely the first power dependence of the concentration, and the qualitative tendency to level off at high concentration.

The concentration dependence of the modulus of gelatin has been reported by Carnali.[10] Data from his Figure 8 are reproduced here in Figure 15 by the square symbols. Some additional data obtained by Bot[43] are shown by the circles. This figure clearly shows that the proportionality $G_N^{(0)} \propto \varrho^{3.1}$, as found in the simulations at lower concentration, holds for gelatin. At a concentration of 5%, the gelatin data show a crossover to a slope of $\sim 1.8 \pm 0.1$, which compares well with the simulation result 1.6 ± 0.2. The simulation results are shown by the crosses, connected by dotted lines. Gelatin is not the only flexible polymer for which the slope ~ 3 is observed at low concentration. The other example discussed by Carnali, guar-gelled by addition of boric acid, shows the same concentration dependence of the plateau modulus over the entire concentration range that was studied.

As a third example we mention the results by Aubry and Moan.[6] They studied the influence of the viscosity on the addition of various amounts of sticking groups to hydroxypropyl-guar. As these polymers contain many association spots that associate into micelles in a reversible way, this system closely resembles the simulation model that was studied here. They reported the zero shear viscosity as a function of the polymer concentration. By 0.3% polymer the viscosity starts to increase roughly linearly in a log–log plot with a slope of 4.1. This closely follows our simulations as the viscosity should scale as $\eta \propto G_N^{(0)}\tau_t \propto \varrho^{3.1}\varrho$; hence we predict a slope 4.1.

5. Discussion and Conclusions

In this section an interpretation will be given for the short-time and the long-time processes that constitute the dynamic modulus, and the comparison with experiments will be summarized into conclusions. We start with the short-time (or high-frequency) ω^n behavior of the modulus. To explain this behavior for polymer systems, we first discuss the (simpler) hard-sphere suspensions. The $\omega^{1/2}$ divergence in these systems can be understood quite easily from the fluctuation–dissipation theorem. The time dependence that appears in eq 13 originates from the (diffusion) Green function. At very short time, all spheres move independently; hence the Green function must be the solution of the free diffusion equation: $\partial G(r,t)/\partial t = D\nabla^2 G(r,t)$. For hard spheres, the divergence of the modulus is caused by the contacts between spheres; hence the decay of the modulus in time is proportional to the number of contacts that have remained after time t. Since only diffusion perpendicular to the surfaces removes these contacts (at contact the spheres are two-dimensional flat surfaces), the decay of stress must be proportional to the solution of the *one*-dimensional diffusion equation at $r = 0$. In arbitrary space dimension d_s, the solution of the diffusion equation is

$$G(r;t) = \frac{1}{(2\pi)^{d_s}} \int e^{ikr - k^2 Dt}\, \mathrm{d}^{(d_s)}k \tag{21}$$

At $r = 0$ (contact) this reduces to

$$G(0;t) = \frac{S(d_s)}{(2\pi)^{d_s}} \int_0^\infty k^{d_s - 1} \mathrm{e}^{-k^2 Dt}\, \mathrm{d}k = \frac{S(\mathrm{d_s})\Gamma(d_s/2)}{2(2\pi)^{\mathrm{d_s}}(Dt)^{\mathrm{d_s}/2}} = \frac{1}{(4\pi Dt)^{\mathrm{d_s}/2}} \tag{22}$$

where $S(d_s) = d_s \pi^{d_s/2}/\Gamma(d_s/2 + 1)$ is the area of a unit sphere in d_s dimensions. Substituting space dimension $d_s = 1$ for interacting (hard-sphere) surfaces, we find the short-time modulus (which must be proportional to the Green function) to diverge as

$$\lim_{t \downarrow 0} G(t) \propto \lim_{t \downarrow 0} G(0;t) \propto t^{-1/2} \tag{23}$$

In the general case where the interacting objects are of d_f (fractal) dimensionality, embedded in three dimensional space, the diffusion process takes place in a $d_s = 3 - d_f$ dimensional space when $d_f \leq 2$. We speculate that for fractal agglomerates of $d_f \geq 2$ this relation also holds, though here we need it only for $d_f < 2$. For polymers, this fractal dimension relates to the swelling exponent as $d_f = 1/\nu$. Accordingly, the modulus at short time must diverge as

$$G(t) \propto t^{-(3-\mathrm{d_f})/2} = t^{-(3/2)+(1/2\nu)} \tag{24}$$

We thus find the divergence exponent n as

$$n = \frac{3 - \mathrm{d}_f}{2} = \frac{3}{2} - \frac{1}{2\nu} \tag{25}$$

On substitution of the swelling exponent $\nu = {}^1/_2$ (θ polymers), we obtain the Rouse behavior $n = {}^1/_2$, $\tan\delta = 1$. When the solvent improves, the swelling exponent increases. Substitution of the Flory exponent[12] $\nu = {}^3/_5$ leads to $n = {}^2/_3$ and $\tan\delta = 3^{1/2}$; the renormalization group value[44] $\nu = 0.588 \pm 0.001$ gives $n = 0.650 \pm 0.002$. Finally, the strong scaling assumption[45] $3\nu = 2 - \epsilon$, combined with the exact enumeration estimate[46] $\epsilon = {}^1/_4$ gives $\nu = {}^7/_{12}$, which leads to $n = {}^9/_{14} \approx 0.643$. Alternative expressions for the exponent n have been given earlier by Martin *et al.*[39] and by Muthukumar.[40] In these analyses relations have come forward between the dynamic exponent n and the fractal dimension d_f, and between n and the percolation exponent k, which describes the viscosity near the sol–gel transition. Martin *et al.* came to the conclusion that $0.66 \leq n \leq 1$ and cited several experiments on gelling polymers where values in the range $0.5 \leq n \leq 0.7$ were observed.

The present theory provides a means to interpret the high-frequency simulation results of section 3. There it was shown that, for the bead-spring model in a

network, the divergence exponent is given by $n = 0.64 \pm 0.01$. Within the simulation error, the same exponent was found for a free chain and for a chain of which some atoms are not allowed to move. Thus it is shown that the high-frequency divergence of the modulus is not related to the fact that a network was formed. Instead, it reflects the movements of a *free* chain, and consequently, the divergence exponent n is determined only by the fractal nature of the polymer chain. Using eq 25, we can translate the *dynamic* scaling exponent $n = 0.64 \pm 0.01$ into the *structural* swelling exponent $\nu = 0.58 \pm 0.01$. This value corresponds well to the expected value $\nu = 0.588$ for (locally) swollen polymers in the blobs. To check this relation explicitly we determined in the same run both $d_f = 1.75 \pm 0.05$ and $n = 0.616 \pm 0.016$. From this fractal dimension, eq 25 predicts $n = 0.625 \pm 0.025$, which compares very well with the independently determined value for this run. Whether or not this fractal dimension analysis is really applicable to our network simulations cannot be checked independently at hard core effects are dominantly present in the structure function of the networks as higher polymer concentration. However, the experience with the present model is that up to concentrations such as $\varrho = 0.26$ thermodynamic scaling relations hold.[22]

The next issue to address is the long-time behavior of the modulus. The question is, how can we understand that the reptation theory seems to fit the results, even though the polymers are not enclosed in a "tube". The tube mechanism clearly does not apply here. What we have here are chains of which the beads follow a hopping motion over a random lattice, where the lattice is formed by the presence of the other beads (i.e., possible association sites). The beads move freely over this lattice, and the hopping frequency is given by the lifetime of the associations. The picture that thus emerges is that of a free polymer chain, which performs a (very slow) diffusive motion. The dissociation of a single sticker does not release all the stress carried by such a chain, but it is only a step toward stress release. The stress carried by such a chain at a given instant is proportional to the square of the end point separation $(r_1 - r_N)^2$. The stress that has *remained* after a certain time is therefore proportional to the dot product between the end point vectors at times 0 and t: $G(t) \propto \langle (r_1(0) - r_N(0))(r_1(t) - r_N(t)) \rangle$. This correlation function can be worked out in the Rouse model [see, for example, Doi and Edwards[11] (p 95)]. Because only the difference between r_1 and r_N is considered, the even modes drop out and $r_1(t) - r_N(t) = \sum_{(p\ \mathrm{odd})} X_p(t)$. Consequently, we find the modulus as[11]

$$G(t) \propto \sum_{p\ \mathrm{odd}} \langle X_p(t) X_p \rangle (0) > \propto kT \sum_{p\ \mathrm{odd}} \frac{8}{\pi^2 p^2} \exp(-p^2 t/\tau) \tag{26}$$

which is precisely the time dependence found in the reptation theory, (eq 18). This alternative model can be accepted as a possible explanation for the long-time correlation, as it does not presuppose the existence of a confining tube, which is clearly nonphysical in the bead-spring simulation model. We feel that the point put forward here is important in the more general discussion on the validity of reptation theory.[47]

As a final point of this discussion we come to the comparison to (bio)polymers, the conclusions, and the predictions. Starting with the (minor) negative points of the bead-spring model: the loss modulus G'' at intermediate frequency decays roughly as $\omega^{-0.45}$. The typical behavior in many experimental systems is that G'' varies with ω to a power -0.4 to $+0.1$. A possible crossover to a more positive power at high association constants runs into practical computer time limitations; therefore, this is difficult to investigate with the present method. A second problem is the fact that at high frequency the modulus in the Hookean bead-spring model is only proportional to $\omega^{0.64}$ (indicating the fractal structure), whereas in real systems the power can increase to higher values. For a more realistic description of the glassy modes, a model of finite extensible polymers has been studied by the same method.[48]

There are several positive points of the bead-spring model; we give a brief summary:

The fact that G'' decays as $\omega^{-0.45}$ is already a substantial improvement over the classical network models like the Green–Tobolsky model that use only the bond length distribution and that predict a $1/\omega$ behavior. The low-frequency fit in Figure 12 is in fact even better than the reptation theory.

The upturn of G' and G'' at high frequency has not been understood even qualitatively with the reptation theory or variations of it that include the tube fluctuations. This upturn did result naturally from the simulation model and could be related to the fractal dimension of the polymers in the blobs. This contrasts with the usual interpretation that hydrodynamic interactions are of dominant importance.

The infinite frequency modulus that experimentally increases roughly linearly with ω is correctly described by the FENE potential model. This gives a first explanation of the finite polymer excess viscosity at high frequency, even *without* the incorporation of hydrodynamic interactions.

The simulations correctly indicate the plateau modulus to scale as $G_N^{(0)} \propto \varrho^{3.1}$, equal to what is found in gelatin and in guar–borate systems. At high concentration the power decreases; the crossover point in the simulations corresponds to the upper binodal density.

The bead-spring model indicates the network relaxation time to scale as $\tau_t \propto \varrho$, in line with the measurements on end-capped PEG systems. Combining the last two points, we predict the zero shear viscosity to scale as $\eta \propto \varrho^{4.1}$, which is in line with experiments on modified guar.

The picture that emerges from the last two points is the following. To interpret the origin of the density dependence of the modulus, we use the scaling relation $G_N^{(0)} \propto \varrho^{3\nu/(3\nu-1)}$. From this relation, we can solve the swelling exponent as $\nu = 1/2$, hence the *elastically active* strands are Gaussian. As was remarked by Annable *et al.*,[5] the fact that the network relaxation time decreases at low concentration means that the active bonds are "superbridges": several polymers are linked together to form a single active chain. If one of the links in this chain breaks the complete connection is lost. Since the probability per unit of time that any of the links of a chain breaks, is proportional to the number of links in the connection, the relaxation time must be inversely proportional to the length of the connection. A short relaxation time thus implies long connections. Indeed, if we estimate the spacial extent of the connections by $R \approx (kT/G_N^{(0)})^{1/3}$, we find $R \approx 0.55/\varrho$. On the other hand, the correlation length of the nonassociating polymers is[22] $\xi \approx (kT/\Pi)^{1/3} \approx 0.6/\varrho^{7/9}$. It is thus seems that the length scale of the connections is larger than the correlation length. On such length scales, however, the

finite volume effects are screened out, and the polymers behave as ideal coils. The shorter relaxation time at low concentration and the third power in the density dependence of the modulus thus have a common origin: the active connections are long superbridges.[5]

To conclude, the bead-spring model may serve as a first model of (weak) polymer gels. Even though the model rests on binary association, the scaling relations also seem to apply to systems with multiple association like gelatin, where the cross-links are most certainly triple helices. The most probable explanation for this fact is that close to the sol–gel transition the dominant effect determining the modulus is the formation of superbridges that are larger than the correlation length. This process is independent of the precise chemical nature of the individual associations, and hence a rather universal behavior can be expected for the complex modulus.

Acknowledgment. The authors thank Dr. Allan Clark for fruitful discussions and Dr Arjen Bot for providing valuable experimental results prior to publication.

References and Notes

(1) Larson, R. G. *Constitutive Equations for Polymer Melts and Solutions*; Butterworth: Boston, 1988.
(2) Heinrich, G. *Prog. Colloid Polym. Sci.* **1992**, *90*, 16.
(3) Sarrazincartalas, A.; Iliopoulos, I.; Audebert, R.; Olsson, U. *Langmuir* **1994**, *10*, 1421.
(4) Magny, B.; Iliopoulos, I.; Zana, R; Audebert, R. *Langmuir* **1994**, *10*, 3180.
(5) Annable, T.; Buscall, R.; Ettelaie R.; Whittlestone, D. *J. Rheol.* **1993**, *37*, 695.
(6) Aubry, T.; Moan, M. In *Progress and Trends in Rheology IV, Proceedings of the Fourth European Rheology Conference*; Gallegos, C., Ed.; Steinkopf: Darmstadt, 1994; p 426.
(7) Edwards, S. F.; Lillford, P. J.; Blanshard, J. M. V. In *Food Structure and Behavior*; Blanshard, J. M. V., Lillford, P., Eds.; Academic Press Ltd.: London, 1987; p 1.
(8) Clark, A. H. In *Food Structure and Behavior*; Blanshard, J. M. V., Lillford, P., Eds.; Academic Press Ltd.: London, 1987; p 13.
(9) Ross-Murphy, S. *Food Hydrocolloids* **1987**, *1*, 485.
(10) Carnali, J. O. *Rheol. Acta* **1992**, *31*, 399.
(11) Doi, M.; Edwards, S. F. *The Theory of Polymer Dynamics*; Clarendon Press: Oxford, U.K., 1986.
(12) de Gennes, P. G. *Scaling Concepts in Polymer Physics*; Cornell University Press: Ithaca, NY, 1979.
(13) Leibler, L.; Rubinstein, M; Colby, R. H. *Macromolecules* **1991**, *24*, 4701.
(14) Pezron, E.; Leibler, L.; Ricard, A.; Audebert, R. *Macromolecules* **1988**, *21*, 1126. Keita, G.; Ricard, A.; Audebert, R.; Pezron, E.; Leibler, L. *Polymer* **1995**, *36*, 49.
(15) Schieber, J. D. *J. Rheol.* **1993**, *37*, 1003.
(16) Wedgewood, L. E. *Rheol. Acta* **1993**, *32*, 405.
(17) van den Brule, B. H. A. A. *J. Non-Newtonian Fluid Mech.* **1993**, *47*, 357.
(18) Grest, G. S.; Kremer, K. *Macromolecules* **1990**, *23*, 4994.
(19) Schultz, M.; Sommer, J. U. *J. Chem. Phys.* **1992**, *96*, 7102.
(20) Kremer, K.; Grest, G. S. *J. Chem. Soc., Faraday Trans.* **1992**, *88*, 1707.
(21) Duering, E.; Rabin, Y. *J. Rheol.* **1991**, *35*, 213.
(22) Groot, R. D.; Agterof, W. G. M. *J. Chem. Phys.* **1994**, *100*, 1649.
(23) Groot, R. D.; Agterof, W. G. M. *J. Chem. Phys.* **1994**, *100*, 1657.
(24) van den Brule, B. H. A. A.; Hoogerbrugge, P. J. In *Progress and Trends in Rheology IV, Proceedings of the Fourth European Rheology Conference*; Gallegos, C., Ed.; Steinkopf: Darmstadt, 1994; p 120.
(25) Groot, R. D.; Agterof, W. G. M. In *Progress and Trends in Rheology IV, Proceedings of the Fourth European Rheology Conference*; Gallegos, C., Ed.; Steinkopf: Darmstadt, 1994; p 90.
(26) Groot, R. D.; van der Eerden, J. P.; Faber, N. M. *J. Chem. Phys.* **1987**, *87*, 2263.
(27) Levesque, D.; Verlet, L.; Kürkijarvi, J. *Phys. Rev. A* **1973**, *7*, 1690.
(28) Green, M. S. *J. Chem. Phys.* **1952**, *20*, 1281. Green, M. S. *J. Chem. Phys.* **1954**, *22*, 398.
(29) Kubo, R. *J. Phys. Soc. Jpn.* **1957**, *12*, 570.
(30) Zwanzig, R. *Annu. Rev. Phys. Chem.* **1965**, *16*, 67.
(31) Zwanzig, R.; Mountain, R. D. *J. Chem. Phys.* **1965**, *43*, 4464.
(32) Heyes, D. M.; Mitchell, P. J. In *Progress and Trends in Rheology IV, Proceedings of the Fourth European Rheology Conference*; Gallegos, C., Ed.; Steinkopf: Darmstadt, 1994; p 657.
(33) van der Werff, J. C.; de Kruif, C. G.; Blom, C.; Mellema, J. *Phys. Rev. A* **1989**, *39*, 795.
(34) Cichocki, B.; Felderhof, B. U. *Phys. Rev. A* **1991**, *43*, 5405.
(35) de Schepper, I. M.; Smorenburg, H. E.; Cohen, E. G. D. *Phys. Rev. Lett.* **1993**, *70*, 2178.
(36) Russel, W. B.; Gast, A. P. *J. Chem. Phys.* **1986**, *84*, 1815.
(37) Brady, J. F. *J. Chem. Phys.* **1993**, *99*, 567.
(38) Durand, D.; Delsanti, M.; Adam, M.; Luck, J. M. *Europhys. Lett.* **1987**, *3*, 297. Lairez, D.; Adam, M.; Raspaud, E.; Emery, J. R.; Durand, D. *Prog. Colloid Polym. Sci.* **1992**, *90*, 37.
(39) Martin, J. E.; Adolf, D.; Wilcoxon, J. P. *Phys. Rev. A.* **1989**, *39*, 1325.
(40) Muthukumar, M. *Macromolecules* **1989**, *22*, 4656.
(41) de Gennes, P. G. *J. Chem. Phys.* **1971**, *55*, 572.
(42) Vilgis, T. A. *Prog. Colloid Polym. Sci.* **1992**, *90*, 1. Jones, J. L.; Marquez, C. M. *J. Phys. Fr.* **1990**, *51*, 1113.
(43) Bot, A. Unpublished results. These data were obtained from a gelatin of another Bloom value and aging time than used in Carnali's experiments. Therefore all moduli have been multiplied by the same overall factor (1.82) to match Carnali's results.
(44) le Guillou, J. C.; Zinn-Justin, J. *Phys. Rev. Lett.* **1977**, *39*, 95.
(45) McKenzie, D. S. *Phys. Rep.* **1976**, *27*, 35.
(46) McKenzie, D. S.; Domb, C. *Proc. Phys. Soc.* **1967**, *92*, 632.
(47) Lodge, T. P.; Rotstein, N. A.; Prager, S. *Adv. Chem. Phys.* **1990**, *79*, 1.
(48) Groot, R. D., to be published.

MA946351D